Downloaded from orbit.dtu.dk on: Apr 20, 2024

DTU Library

Cryo-temperature effects on membrane protein structure and dynamics

Mehra, Rukmankesh; Dehury, Budheswar; Kepp, Kasper Planeta

Published in:
Physical Chemistry Chemical Physics

Link to article, DOI:
10.1039/c9cp06723j

Publication date:
2020

Document Version
Peer reviewed version

Link back to DTU Orbit

Citation (APA):
Mehra, R., Dehury, B., & Kepp, K. P. (2020). Cryo-temperature effects on membrane protein structure and dynamics. *Physical Chemistry Chemical Physics*, *22*(10), 5427-5438. https://doi.org/10.1039/c9cp06723j

General rights
Copyright and moral rights for the publications made accessible in the public portal are retained by the authors and/or other copyright owners and it is a condition of accessing publications that users recognise and abide by the legal requirements associated with these rights.

- Users may download and print one copy of any publication from the public portal for the purpose of private study or research.
- You may not further distribute the material or use it for any profit-making activity or commercial gain
- You may freely distribute the URL identifying the publication in the public portal

If you believe that this document breaches copyright please contact us providing details, and we will remove access to the work immediately and investigate your claim.

Cryo-temperature effects on membrane protein structure and dynamics

Rukmankesh Mehra, Budheswar Dehury and Kasper P. Kepp*

DTU Chemistry, Technical University of Denmark, DK-2800 Kongens Lyngby, Denmark

*Corresponding author. E-mail: kpj@kemi.dtu.dk. Phone: +045 45252409

ORCIDs

RM: 0000-0001-6010-1514, KPK: 0000-0002-6754-7348

TOC entry

Cryo-electron structures revolutionize biology, yet cooling effects are unclear. We developed a simulation protocol studying hot, cold, and rapidly cooled γ-secretase (6IYC). We identify cryo-contraction and frozen modes relevant to Aβ production and cryo-analysis in general.

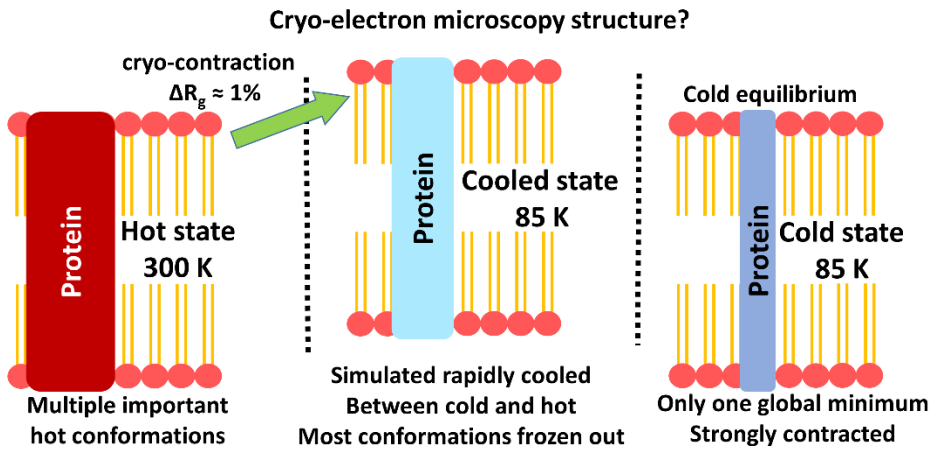

Abstract

Innovations in cryogenic electron microscopy (Cryo-EM) have led to high-quality structures of important proteins such as the ribosome and γ-secretase, the membrane protease that produces Aβ involved in Alzheimer's disease. However, freezing may change protein structure and dynamics relative to the physiologically relevant "hot" state. To explore this, we studied substrate-bound γ-secretase (6IYC) by molecular dynamics as a hot, cold, and quickly cooled state in both membrane and water systems. We show that the experimental structure resembles the simulated cooled state, structurally between the hot and cold states and membrane and water systems, but with cold dynamics. We observe "cryo-contraction" in the membrane from 303 to 85 K, reducing radius of gyration (R_g) by 1% from 4.01 to 3.97 nm (6IYC = 3.95 nm). The hot state features an unwound C83-substrate with 10-14 α-helix residues (6IYC: 11) in equilibrium with an intact state with 16 helix residues not previously reported. The β-sheet is weakened with temperature. Multiple hot conformations probably control the $A\beta_{42}/A\beta_{40}$ ratio. We thus propose that MD simulation protocols of hot, cold, and cooled states as proposed here can correct cryo-EM coordinates. However, important frozen-out fast modes require specific supplementary hot simulations or experiments.

Keywords: Cryo-electron microscopy; cryo-contraction; molecular dynamics; membrane protein; γ-secretase

Introduction

Protein structures derived from cryogenic electron microscopy play an increasing role in structural biology due to recent technical innovations relating to improved electron detectors, sample handling, and image processing[1–4]. Sample ionization by the electrons increases with temperature, and thus measurements are done at low temperature[5]. Typical samples consist of protein molecules with a layer of amorphous (vitreous) ice on a perforated film, rapidly cooled using a cryo-agent such as liquid ethane[1,3]. 2D-images of the sample at different orientations are combined for 3D-reconstruction of the protein structure, either by single particle analysis[4] or subtomogram averaging[3].

Membrane-embedded proteins are particularly difficult to purify in water due to their hydrophobic transmembrane domains. Detergents stabilize them but complicate crystallization. Cryo-EM of membrane proteins is thus very important, as the technique circumvents the crystallization problem. Cryo-EM can capture proteins solubilized in detergents or amphipols [6], or stabilized in the saposin-lipoprotein system[7] or the nanodiscs[8], which may resemble biological membrane environments.

Most emphasis has been on sample preparation, electron detectors, and image processing; the temperature effects on protein structure and dynamics tend to be ignored[2,3]. Ironically, the need to freeze atoms to avoid ionization damage at the same time removes potentially important motions of the protein[9–12]. It is tacitly assumed, and never discussed in any of the major published cryo-EM structure papers, that the cooling rate after immersion into the cryo-agent is so fast that the system retains the ensemble-average structural properties of the hot state, and that the relevant ensemble of conformations may be obtained from image analysis.[13]

Protein dynamics are not well understood below water's freezing point[9]. Sample freezing influences morphology and causes micro-heterogeneity[14]. Properties of the cooled sample depend on concentration, protein, the method and rate of cooling, and the degree of super cooling[15–20]. Protein structure and dynamics is crucially affected by water, which displays a remarkable diversity of temperature-dependent structural dynamics, which a clear distinction between bulk water and water at the protein surface[11]. The glass transition of amorphous water is very dependent on cooling rate and can effect protein structure[11]. Infrared O-H vibration spectroscopy of water in cooled myoglobin films indicates a state between liquid water (hot state) and amorphous ice[11].

Because typical freezing rates of seconds or minutes are slower than the sub-second timescale of most conformational changes[21], finite cooling rates tend to freeze out important conformations, leaving only cryo-contracted states with lowest free energy[9–11]. Temperature-variable X-ray diffraction indicates systematic differences between cryo- and ambient temperature which may affect the biological relevance[12,22]. For most proteins where cryo-EM is the method of choice, conformational changes are notable and commonly important to function. This poses a dilemma that warrants systematic analysis.

To explore this problem, we report systematic studies of the structure and dynamics of γ-secretase at cryo- and ambient temperature, using molecular dynamics (MD) computer simulations. γ-secretase is the important membrane protease responsible for producing β-amyloid (Aβ) involved in Alzheimer's disease (AD); conformational changes are suggested to be particularly important to this protein in relation to Aβproduction[23–25], and thus we consider the protein an ideal test case for thermal effects on protein conformations. The paper is the first to study cryo-temperature effects on a membrane protein to our knowledge. Such comparisons are not experimentally feasible due to radiation damage at high temperature, whereas simulations describe the exact same species and composition at infinite resolution.

Due to the resolution, cryo-EM signatures of local structure are weak for residues with low structure propensity whose structural transitions ironically are particularly important, and thus, although not widely appreciated, need molecular calculation for confirmation. As an example of this, the much heralded sheet signal in the original data[24] is in fact quite weak, with many programs (such as Maestro) failing to notice it; DSSP recognizes only six residues as having strand, whereas nine were stated in the paper[24], and the much debated three-residue strand of C83 involved in the recognition motif is not discovered by the state-of-the-art DSSP algorithm at all. APP-C83 may bind more strongly than APP-C99 and thus induce sheet whereas APP-C99 does not. The experimental structure represents a mutant enforcing APP-C83 substrate binding, which could also increase the association and sheet tendency of the complex.

We studied the 6IYC system of γ-secretase[24] at physiological temperature (hot state; 303 K), liquid nitrogen temperature (cold state; 85 K) and in a rapidly cooled state. In general, the 6IYC structural parameters resembled closely to the cooled state that we simulate, providing confidence in the quality of the approach. We then show that the 6IYC and cooled state differ substantially from the hot state that they are supposed to mimic. We find that many structural properties of the cooled state resemble those of the hot state, whereas the dynamics mainly resemble the cold state. We quantify the cryo-contraction of γ-secretase for the first time, which

affects both the radius of gyration and the solvent accessible surface area of the protein, and show that the contraction is larger in the membrane than in water. Importantly, in the cooled state, these two properties are intermediate between the hot and cold states and comparable to the experimental 6IYC structure. The effects are fully consistent with X-ray diffraction studies at variable temperature for myoglobin and ribonuclease[10] and myoglobin[11], but the magnitude of the effects are specific to γ-secretase.

Methods

Models and system set-up

We studied the recently published cryo-EM structure of γ-secretase with the substrate APP-C83 bound (PDB code 6IYC, resolution 2.6 Å) elucidated using single-particle analysis (**Fig. 1a**)[24]. The sample was prepared at 4°C and transferred to liquid nitrogen (~80-85 K) for data collection[24]. The structure contains five protein chains (the four subunits nicastrin, presenilin 1, APH1A, PEN2 and the substrate analog APP-C83) along with heteroatoms of N-acetyl-D-glucosamine, beta-D-mannose, 1,2-diacyl-sn-glycero-3-phosphocholine, and cholesterol. The most interesting feature of this structure is a widely discussed anti-parallel three-stranded β-sheet "recognition motif" of PS1 and APP-C83, which was not seen in the apo-protein structure[23], and a partial unwinding of the helix of transmembrane APP-C83, which may help to explain how the natural substrate APP-C99 becomes hydrolyzed to form Aβ. The structure contains mutations Q112C/D385A in PS1 and V695C in APP-C83, which stabilized the γ-secretase-APP-C83 complex by disulfide crosslinking.

The heteroatoms in 6IYC were removed using BIOVIA DSV[26], missing side chains were added using the WHAT-IF web server[27], and the mutations (Q112C/D385A in PS1) were converted to wild-type using PyMOL[28] and energy minimized using BIOVIA DSV[26]. The fragment containing other mutation V695C in APP-C83 is absent in the structure. The protonation states were prepared at pH 7.4. The catalytic Asp-257 and Asp-385 were both deprotonated as widely assumed experimentally and in accordance with their pK_a; this was further confirmed using PROPKA calculations both with and without membrane at both pH 6, 7, and 8; only at pH 5 did a protonated state appear for the enzyme complex.

The membrane system (containing protein, membrane, water, and salt as the major components) was constructed by orientation of the protein in 1-Palmitoyl-2-oleoylphosphatidylcholine (POPC) bilayer coordinates using the PPM server[29]; the membrane was built using the CHARMM GUI server[30]. The 6IYC structure was optimized, and the POPC membrane and water molecules were added to the system, as shown in **Fig. 1a** (the number of atoms in each system is given in **Supplementary Table S1**). 0.15 M NaCl was applied in the form of Na^+ and Cl^- ions using Monte Carlo randomization. The files generated by CHARMM GUI[31] were used as input to the GROMACS molecular dynamics program[32,33]. These constitute the energy minimization followed by a default six-step pre-equilibration protocol. The pre-

equilibration included first two instances of temperature coupling for 25 ps with a time interval of 1 fs, followed by two steps of temperature and pressure coupling (25000 x 1 fs) and finally two phases of 50000 x 2 fs, each at constant temperature and pressure. The Berendsen method[34] was used to maintain temperature and pressure during membrane system equilibration. Parameters and topology were assigned according to the CHARMM36 force field[35] and TIP3P water[36], which was used for simulation.

We also simulated a water system (containing protein and TIP3P water) to understand the cryo-effects that are distinct to the membrane in context to those expected without the presence of membrane. This system was prepared using the CHARMM GUI server and included 0.15 M of NaCl as randomly placed Na^+ and Cl^- ions using Monte Carlo sampling. The prepared system was minimized and equilibrated using 25 ps temperature coupling with the Nose-Hoover thermostat at a time interval of 1 fs[37].

Molecular dynamics simulations

To understand the effect of temperature and cooling separately, we devised a simulation protocol as follows: We studied the cryo-EM structure in different thermal states: hot, cold and cooled. The hot state is the protein consistently at 303 K, the cold state is consistently at 85 K, and the cooled state was started from the representative hot-state-equilibrated-structures obtained from cluster analysis, subsequently simulated immediately at 85 K, i.e. with "infinite" cooling rate. There is strictly speaking one time step between them, but as little atomic motion occurs on a 1 fs time scale of relevance to experimental cooling rates, this is a good model of practically infinite cooling rate that we can recommend in future studies. 85 K is a reasonable, estimated effective temperature of a cryo-EM sample cooled by liquid nitrogen (boiling point 77 K). Errors in the sampling and force field quality, which generally affect MD accuracy, largely cancel when comparing the system at different temperature, as shown below, in contrast to standard MD studies of "absolutes" that have much larger errors if not designed to eliminate the inherent systematic errors.

The production simulations were performed for 500 ns with a time-step of 2 fs. All simulations were performed in triplicate, using random velocity seeds to initiate three independent simulations for each membrane and water system at 303.15 K and 85 K. Clustering was performed using the method by Daura et al. implemented in Gromos with 0.2 cut-off[38], and the representative structure of the final 300 ns of each 303-K simulation was used as input

for three new simulations at 85 K. Thus, in total 15 simulations (5 states studied in triplicate) were performed, each for 500 ns. The Nose-Hoover algorithm[37] was used to maintain temperature and the Parrinello-Rahman method[39] was used to maintain the pressure of the system. The Verlet cut-off scheme[40,41] was used for all the minimization, equilibration and production steps in both the water-membrane-protein and water-protein systems.

Analysis of membrane and water systems

The membrane and water parameters of the simulation systems were analyzed over the full trajectories[32,42]. We calculated the partial densities of the POPC membrane groups (head, tail and phosphate groups) and TIP3P water. The deuterium order parameters of the sn1 and sn2 tails of POPC were identified, providing the time-averaged orientation of the bonds in the lipid chains and therefore, the angular fluctuations around the bilayer normal. The membrane area, area per lipid, and membrane thickness were calculated using FATSLiM program[42].

Analysis of structure and dynamics

The root-mean square deviation of the structure from its starting configuration (RMSD), the radius of gyration (R_g), and solvent accessible surface area (SASA) were obtained over the full simulated trajectories of all 15 systems. The RMSD values were calculated for the backbone atoms. The root-mean square fluctuations (RMSF) of the protein Cα atoms, secondary structure analysis of the C83 and PS1 subunits, principal component analysis (PCA) and contact analysis were performed using the final equilibrated trajectories from 200-500 ns. The PCA involves building the covariance matrix of the atomic fluctuations and diagonalizing it. The resulting eigenvectors with their corresponding eigenvalues (nm^2) describe the collective modes of motion of the protein. The eigenvectors with the largest values (EV1 and EV2) represent the most significant of these collective motions, and were analyzed in particular detail.

Results and discussion

Membrane-protein-water dynamics at variable temperature

Experimental cryo-EM samples of membrane proteins represent a composition intermediate between a solvated membrane protein and a protein in amorphous ice, with layers of both lipids and frozen water surrounding the protein molecules on the film[3,4]. Since this poorly defined composition may affect the temperature-dependencies of the protein ensemble, we studied γ-secretase both in a complete membrane-water system and in water alone as the two extrema of such compositions, both at 303 K and at 85 K. In addition to these four systems, we also studied the complete wild-type protein-water-membrane system (**Fig. 1a**) at infinite cooling rate as the best-possible sample preparation benchmark of cryo-EM with an intact membrane and without mutation to enforce substrate binding. We aim to determine how this best-possible cooled system with precise chemical composition differs from the cryo-EM structure, and how the temperature and membrane contributes to differences.

Before analyzing the 15 protein-water and protein-water-membrane systems at variable temperature, we first tested the consistency of the overall protein-membrane system. Since the full membrane coordinates are not present in 6IYC, we validated our equilibrated membrane structure against known deuterium magnetic resonance lipid order parameters of the POPC bilayer[43]. The sn1 (the terminal CH_2 carbon of the triglyceride backbone to which palmitic acid is attached) and sn2 (the middle CH carbon) positions of POPC molecules in the membrane and the deuterium order parameters were calculated as shown in **Fig. 1b**. In the hot state, the calculated order parameters are in excellent agreement with the experimental values for POPC [43], with both experimental and computed Sn1 parameters showing a minimum at the third carbon, a maximum at carbon 5-6, and then a monotonic decrease along the palmitoyl chain, and Sn2 parameters showing a double hump structure with a minimum at carbon 10 of the oleoyl chain, i.e. the modeled hot membrane ensemble is very accurate.

The cold state has a very distinct ensemble-averaged membrane structure, with disturbed orientations of the Sn1 chain in particular for the first, most buried atoms, where membrane disorder is largest. We also show that the cooled state, representing the best possible cryo-EM sample with a full intact membrane, exhibits order parameters similar but not identical to the hot state with orientation changes of ~10% estimated from the deuterium order parameters.

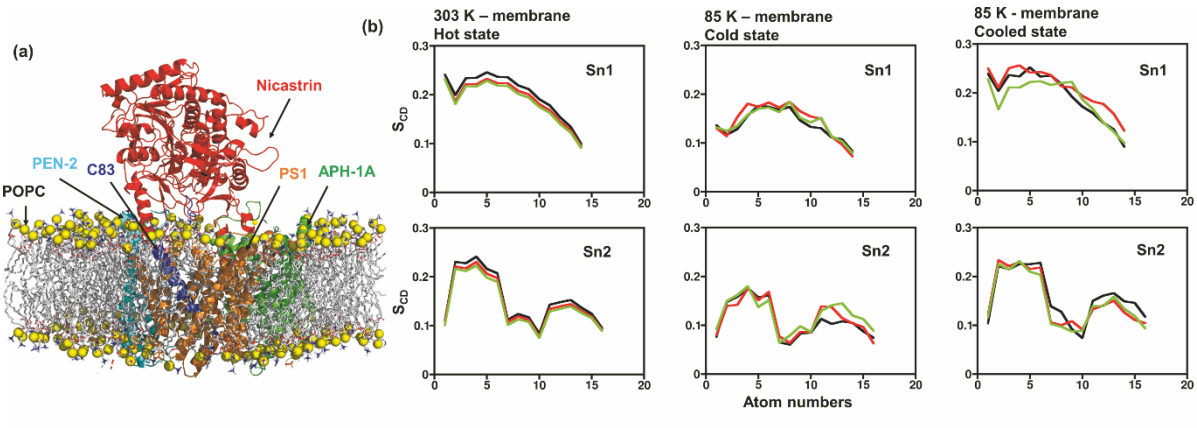

Fig. 1 Analysis of the membrane and water systems during 500 ns simulations of the hot cold and cooled states. The black, red and green colors represent the three independent simulations for each protein state. These color codes are used throughout the article. **(a)** Representation of γ-secretase (6IYC) in POPC membrane system. **(b)** Deuterium order parameters for each atom of the sn1 and sn2 chains of POPC.

The detailed partial densities of the head, tail and phosphate groups of the membrane and water molecules are summarized in **Supplementary Fig. S1** and **S2**. The hot and cold states of the protein-membrane-water system showed distinct distributions of these groups (**Fig. S1**), whereas the cooled state displayed head, tail and phosphate group densities intermediate between those of the hot and cold states. In addition, the total area, thickness, and area per lipid of the simulated membranes are shown in **Supplementary Fig. S3**.

These observations together show that the cooled state resembles but is not identical to the hot state, because it has retained some of the features unique to the cold state. The notable differences between the three states rationalizes the need for considering all three together. The origin of the differences (discussed below) relates to the partial freezing out of some, but not all modes of the hot state in the cooled state, whereas the cold state represents complete freezing out of all membrane-protein-water modes, leaving only the global free energy minimum state. These differences illustrate that even the best-possible cryo-EM sample produced with infinite cooling rate differs in its membrane structure by about 10% from the hot state, if the membrane is complete. The differences may be significant in terms of local protein-membrane interactions relating to protein function. Thus, we recommend that future cryo-EM studies of membrane proteins study both the hot and cooled states using the MD protocol that we propose here, after validating its consistency against the experimental Sn1 and Sn2 deuterium order parameters.

Structural variations in cold, hot, and cooled protein-membrane-water systems

To understand in detail the structural variations in the respective ensembles, we computed the RMSD relative to the starting structure of each simulation of both the membrane and water systems in the hot and cold states (**Fig. 2a-2e, Fig. S4a,** and **Tables 1** and **S2**), as well as the radius of gyration (R_g, in nm) and solvent-accessible surface area of γ-secretase (SASA, in nm^2). As expected, the hot states of both the protein in the membrane and in water display the typical type of thermal structural variation. Structural variations (RMSD) were larger for γ-secretase in water (**Fig. 2d**) than in the membrane (**Fig. 2a**), showing that the membrane consistently dampens the structural variations of the protein, due to the steric enforcement by the lipid molecules. In the cold and cooled states, these variations are greatly reduced at 85 K (**Fig. 2b, 2c, 2e**).

We now discuss the cryo-contraction. The experimental (6IYC) R_g is ~3.95 nm, as shown by blue dashed lines in **Fig. 2**. Importantly, the membrane-enforced restriction at 303 K discussed above occurs from a substantially expanded protein state in the membrane (R_g = 4.01 ±0.03 nm averaged over the three ensembles, **Fig. 2a middle, Fig. S4b** and **Tables 1, S2**) compared to water (R_g ~ 3.93 nm, **Fig. 2d middle**). The experimental value (3.95 nm) is intermediate between these, consistent with its intermediate lipid-water composition, but it is closest to the lipid-free state, indicating that some but not all of the lipid environment is lost in the film.

Cryo-contraction has been estimated from temperature-dependent X-ray diffraction to amount to 0.4% volume contraction per protein molecule per 100 K for ribonuclease in the relevant temperature range from 98 to 320 K[10]. For γ-secretase, we obtain from our simulations a cryo-contraction in water from 3.93 nm to 3.83 nm in the equilibrium cold state (**Fig. 2e, right**), about 2.5%, using R_g as defining property. In the membrane, the contraction from hot to cold state is 5% (4.01 to 3.80 nm), whereas the cooled state is contracted by 1% to 3.97 nm. Both these cryo-contractions are clearly outside the standard deviation of our triplicate simulations, and is further supported by the excellent agreement between R_g of 6IYC (3.95 nm) and our simulated cooled state (3.97 nm) (**Fig. 2c middle**), in particular when considering the membrane expansion effect accounting for some of the small increase relative to the real sample, which is a mixture of lipids and water on a film.

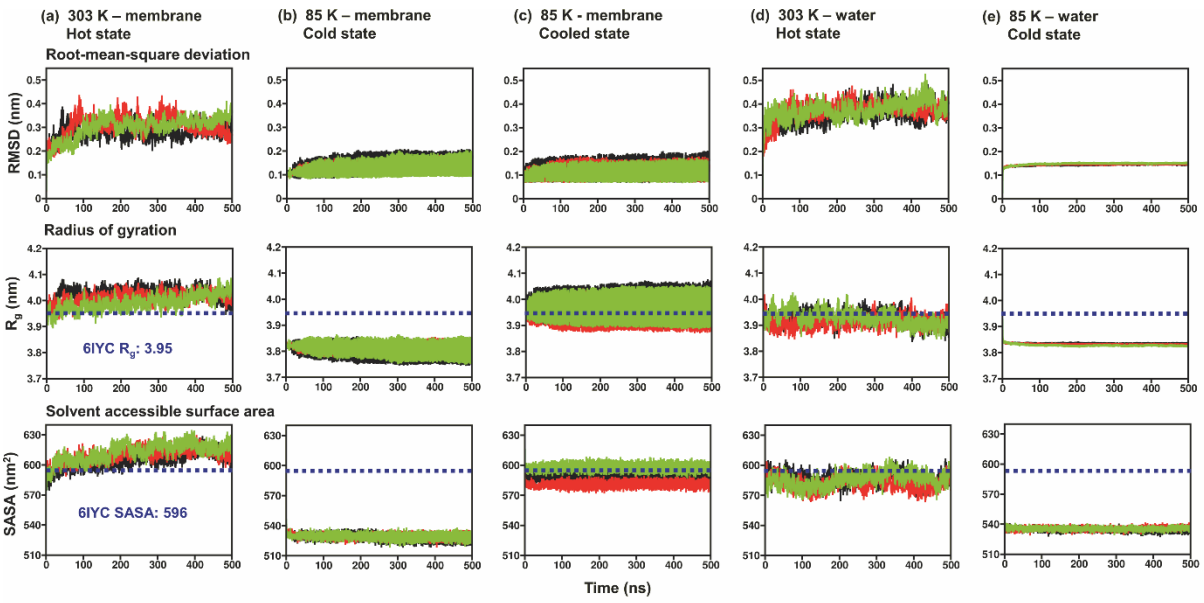

Fig. 2 The RMSD, radius of gyration (R_g), and solvent accessible surface area (SASA) during 500 ns of MD simulation. Blue dashed lines indicate experimental values (6IYC). The black, red and green colors represent three independent simulations of each state. **(a)** Hot state of protein in membrane. **(b)** Cold state in membrane. **(c)** Cooled state in membrane. **(d)** Hot state in water. **(e)** Cold state in water.

Consistent with the R_g, we found that the SASA also increased with temperature by ~50 nm^2 in the water state and by typically ~80 nm^2 in the membrane state, i.e. the exposed surface is substantially reduced at cryo temperature and much more so in a membrane (**Fig. 2, row 3, Fig. S4c,** and **Tables 1, S2**). R_g significantly correlates with SASA (R^2 = 0.1−0.8, **Table S3**). Better correlation was observed for membrane than water systems, and for the cold and the cooled membrane states (R^2 = 0.6−0.8) compared to the hot state (R^2 = 0.1−0.3). The SASA of our simulated cooled membrane state is in excellent agreement with the value for 6IYC, further confirming that this state closely resembles the relevant temperature state of the experimental system, but with more explicit membrane composition. Thus, the experimental cryo-EM structures do not suffer strong structural artefacts of the cold state, but the cooling still removes some motions from the protein that contribute to overall variation in hot-state structure, surface area, and size. This difference between the cryo-EM structure and the physiologically relevant hot state is enforced by the membrane.

We further analyzed R_g and SASA of each γ-secretase subunit separately (**Supplementary Tables S4, S5** and **Figures S5, S6**). Nicastrin and PS1 undergo the largest thermal expansion

of the four subunits. The large non-spherical structure of the protein is mainly enforced by nicastrin and contributes the most to the cryo-contraction that we identify. In all cases, the cooled state values are intermediate between the hot and cold states and close to the experimental 6IYC structure as expected. However, we notice that the C83 cold state resembles most the 6IYC, probably because this small peptide has the fastest time scales. C83 shows significant expansion with temperature, directly relevant to its cleavage, since the combined effect of membrane and temperature substantially affects active site space (see below). In terms of convergence, the generally horizontal behavior of most trajectories in **Figure 2** emphasize stable ensemble useful for statistics, but not strictly "convergence, which is very hard to prove. Instead, **Tables S2** and **S4** show the actual averages and standard deviations for the properties of main interest to our work and show that these variations in averages are significant relative to the variations, which is our most robust way of confirming the significance.

Similar to R_g, SASA increased the most for nicastrin and PS1, and the cooled state was also in this regard intermediate between the hot and cold states and most similar to 6IYC (except for C83 as noted above). R_g and SASA of individual protein subunits correlate (**Supplementary Table S6**), with cooled state showing highest correlation. In contrast, the cold water-protein state did not show strong correlation between the two properties (R^2 = 0.02-0.1).

Very few studies have explored the effect of cryo-contraction, yet our findings are fully consistent both with the experimental structure[24], with general temperature effects on proteins[10,11], and with the different structural and dynamics properties of the water and membrane protein systems studied. In fact, our estimated 1% cryo-contraction is very similar to that obtained by Tilton Jr. et al.[10] The root-mean-squared structural fluctuations confirm this picture and provide details on the motions that contribute the most to the overall dynamics of the γ-secretase subunits (**Fig. S7**). From a dynamic perspective, the cooled states resemble the cold states with similar, small fluctuations occurring at 85 K, but as discussed above, these dynamics importantly occur in different free energy landscapes, with the cold state having frozen out all conformations except the global minimum, whereas the cooled state having frozen out the dynamics of only the fast modes in each free energy basin.

In the present study, we used the cryo-EM structure (6IYC) without modeling the missing parts to avoid computational pollution of the coordinates. In order to analyze whether the missing parts in 6IYC (such as missing loop between TM6-TM7 and presence of C83 instead of C99) could explain some of the thermal differences, we compared R_g and SASA of the hot state in membrane with previous structures at 303 K of complete γ-secretase-C99 complex in a

membrane-water system (**Table S7** and **Figure S8**)[44]. Whereas the R_g and SASA are of course larger in the complete model because of the presence of the loop, we find that the hot state dynamics are very similar in the parts that are the same, where they can be compared, and thus these changes do not change the thermal effects on the "remaining" visible part of the conformations and dynamics seen in 6YIC that are the main topic of the present work.

Table 1 Average values (standard deviations) of the simulated properties; averaged from triplicate independent simulations of each temperature for the membrane-protein-water and protein-water systems.

Property	**303 K - membrane Hot state**	**85 K - membrane Cold state**	**85 K - membrane Cooled state**	**303 K - water Hot state**	**85 K – water Cold state**
RMSD (nm)	0.30 (0.04)	0.13 (0.03)	0.11 (0.03)	0.37 (0.04)	0.15 (0.005)
R_g (nm) (6IYC = 3.95)	4.01 (0.03)	3.81 (0.03)	3.97 (0.05)	3.92 (0.03)	3.83 (0.003)
SASA (nm^2) (6IYC = 596)	609 (8)	529 (3)	589 (4)	585 (6)	535 (2)
C83 α-helix (6IYC = 11)	13 (2)	14 (1)	14 (1)	15 (1)	15 (1)
PS1 β-strand (6IYC = 6)	2 (2)	2 (0)	2 (0)	2 (1)	5 (2)
Asp257-Asp385 (nm) (6IYC = 1.06)	1.15 (0.04)	1.04 (0.01)	1.14 (0.02)	1.46 (0.06)	1.08 (0.01)
C83-PS1 H-bonds	10.28 (1.97)	10.60 (0.43)	9.95 (0.48)	6.67 (1.60)	9.71 (0.52)

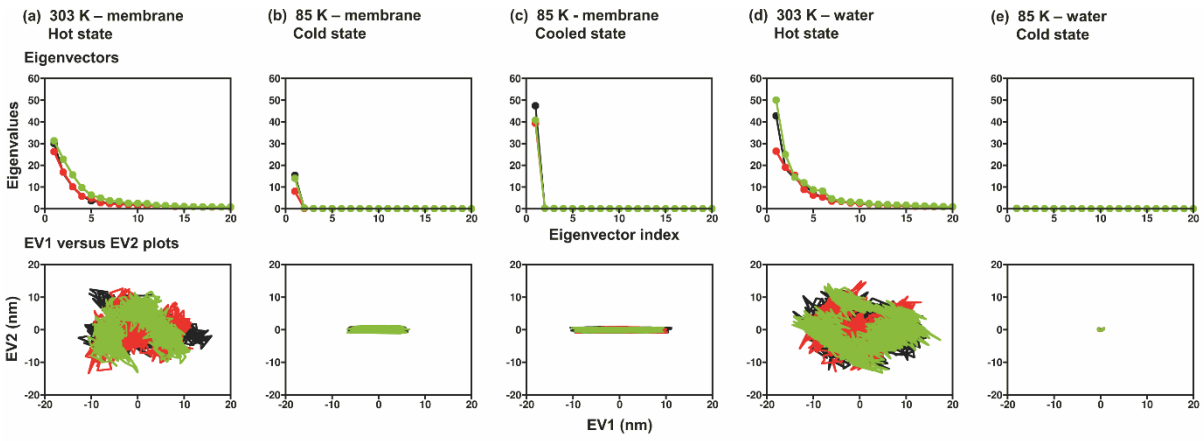

Fig. 3 Principal component analysis on the final 300 ns trajectories and the eigenvalue (nm^2) versus eigenvector plots, and eigenvector 1 (EV1) versus eigenvector 2 (EV2). (a) Hot state of protein in membrane. **(b)** Cold state in membrane. **(c)** Cooled state in membrane. **(d)** Hot state in water. **(e)** Cold state in water.

Cooling effects on γ-secretase free energy landscapes

As shown above, the experimental cryo-EM state resembles closely an infinitely cooled state as computed by MD with a composition between membrane and water. Accordingly, it is distinct from the hot state both structurally and dynamically, as this could affect the conclusions on structure-function relations based on the cryo-EM structure. The most important of these relate to the conformational states of γ-secretase, which explain how the protein produces Aβ peptides of variable length via states of looser or stronger affinity or "grapping", i.e. the Fit-Induce-Stay-Trim (FIST) model[45]. In terms of the cryo-EM structure, emphasis was on the reduced helix content of the bound substrate indicating a partial unwinding of the helix that could explain how peptide bonds become exposed to the catalytic aspartates to enables cleavage, and the β-sheet recognition motif, which was not present in the apo-structures[24].

To understand how temperature, cooling, and membrane lipids affect the conformational landscape, we analyzed the conformational space of γ-secretase using PCA, as summarized in **Fig. 3**, which shows the most important PCA eigenvectors for the five different systems. The number of eigenvalues required to describe the protein clearly depend mainly on temperature, with the membrane hot state (**Fig. 3a**) having many more important eigenvectors than the membrane cold state (**Fig. 3b**) and cooled state (**Fig. 3c**). The membrane makes the conformational space more diverse in at least two of the three independent simulations. Thus, one simulation in water (red) represents a more entropic state whereas the two other water states

(green/black) are less entropic (**Fig. 3d**), but in the membrane, all three states are entropic (**Fig. 3a**). The water cold state serves as reference state with almost zero entropy, all modes completely frozen out, and thus no meaningful PCA (**Fig. 3e**).

The plots of EV1 and EV2 show the sampled conformations of the subspace along these eigenvectors, with each point representing a single snapshot of a simulation (**Fig. 3 bottom**). The multi-state nature of the γ-secretase hot state is evident in both water and membrane but cooled γ-secretase, whose structural properties are in excellent agreement with 6IYC only represents a broad single state with correlating motions frozen out. Since the conformational variation in γ-secretase is central to function, it is essential that the cryo-EM structure is supplemented by explicit accounts of atomic dynamics, as attempted in the present work.

The clustering analysis (**Supplementary Table S8**) produces the largest number of important clusters for the hot water-protein state (61±9 clusters). For the hot membrane-protein-water state, 22±4 clusters were required to describe the conformational structure of the protein. For the cold and cooled states, only one cluster per simulation was required, consistent with the complete freezing out of alternative conformation states, and showing clearly that the membrane dampens the conformational variation of the embedded protein.

Secondary structure analysis

The secondary structure of the substrate analog C83 has been a major focal point in the new cryo-EM structure, as its partial unwinding could indicate a mechanism of access to the peptide bonds of the substrate that are cleaved by the protease[24]. We have previously studied wild-type γ-secretase in membrane-water systems both with and without the natural substrate APP-C99 bound[44,45]. While we initially observed β-strand propensity of presenilin[46], we have failed to reproduce β-sheet at ambient temperature in a complete membrane-protein-APP-C99-water system[44]. To understand how temperature and membrane content affect this helix unwinding, we analyzed the number of residues forming α-helix in C83 in all simulations (**Fig. 4, S4d** and **Tables 1, S2**). We also compared the number of residues with unusual strand structure in PS1, which has been argued to be involved in a recognition motif with the substrate analog C83[24].

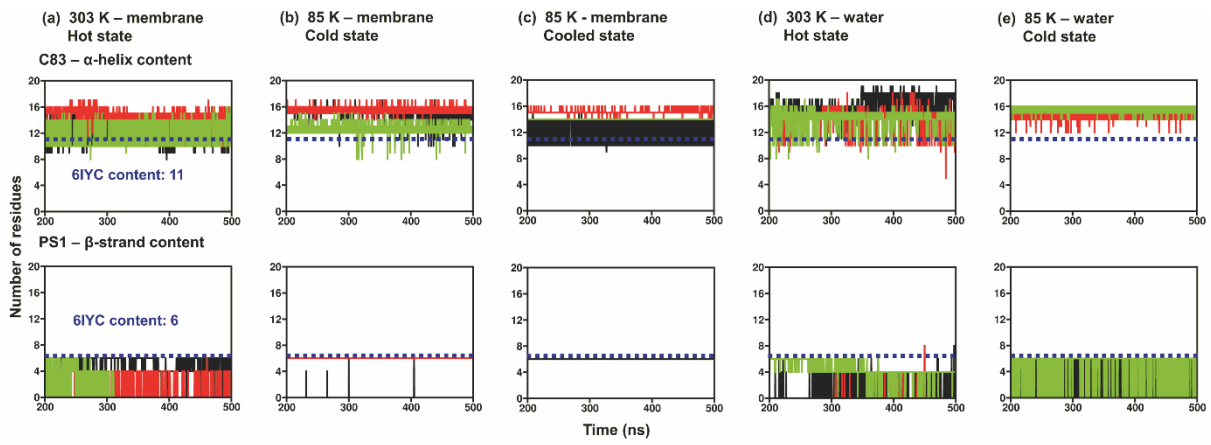

Fig. 4 Number of residues forming α-helix in the substrate C83 and β-sheet in the catalytic subunit PS1 of γ-secretase. The dashed blue line represents the secondary structure content of the experimental 6IYC structure. **(a)** Hot state of protein in membrane. **(b)** Cold state in membrane. **(c)** Cooled state in membrane. **(d)** Hot state in water. **(e)** Cold state in water.

Starting with C83 helix, the experimental 6IYC structure (shown in blue dashed lines in **Fig. 4, row 1**) contains 11 residues with α-helix structure when using the DSSP algorithm in Gromacs. The results show that the hot membrane state (**Fig. 4a**) enables the most prevalent C83 helix unwinding, with experimental value of 11 residues being representative to the lower side within the black and green ensembles. In contrast, the cold states tend to contain more helix structure, staying mainly in the higher end of the interval at 14-16 helix residues (**Fig. 4b, 4e**). In contrast, the cooled ensemble consists of several conformations of C83 (**Fig. 4c** and **Supplementary Table S2**)[24]. The 6IYC structure represents only one of these conformations with 10-14 residues, whereas the intact helix conformation with 16 helix residues is not evident from 6IYC. The high helix content in different states could be because of the force field uncertainty as previously reported[47–49]. However, the cooled state contains both unwound and intact conformations in the same ensemble in thermal equilibrium.

Although reversible winding-unwinding occurs also in the cold states (**Fig. 4b, 4e**), only the hot states favor unwinding consistently, as the thermal energy facilitates the breaking of helix hydrogen bonds. We also find that the membrane plays a key role in stabilizing the unwound conformation state (green, **Fig. 4a**), whereas the same state only rarely unwinds in the water ensemble (**Fig. 4d**). Thus, both temperature and the membrane are integral for enabling the unwinding of 2-3 residues of C83 to expose the peptide bond. In addition, C83 does not form any β-strand when measured by DSSP (in Gromacs 2018.5), in full accordance

with the fact that such strand is not recognized by DSSP in 6IYC. This strand along with the two PS1 strands was visualized as forming anti-parallel β-sheet in 6IYC, which may be possible with some programs such as PyMOL[24]. Consistent with this, previous important work has shown that the membrane composition plays a significant role for the dynamics of γ-secretase and potentially C99 cleavage to form Aβ.[50–52] Our effects are smaller, probably because we study thermal effects on a direct background of the experimental 6IYC structure, to avoid computational divergence towards other features, but while our emphasis is on separating out the thermal effects, the combined works show that both thermal and membrane effects are important for γ-secretase dynamics and to some extend correlate.

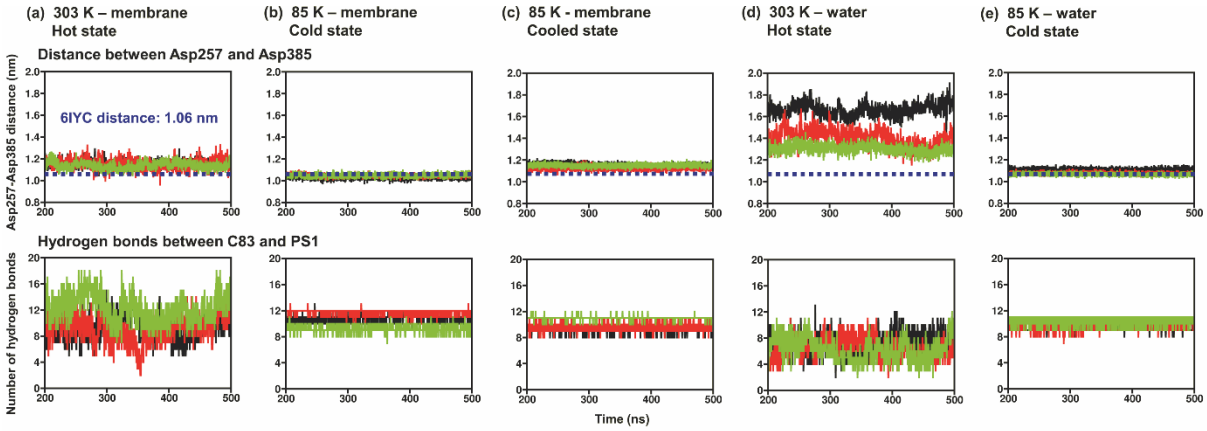

Fig. 5 Catalytic Asp257-Asp385 distances and the number of hydrogen bonds between C83 and PS1. (a) Hot state of protein in membrane. **(b)** Cold state in membrane. **(c)** Cooled state in membrane. **(d)** Hot state in water. **(e)** Cold state in water. Blue dashed lines show the corresponding values for the cryo-EM structure 6IYC[24]. For plots that overlap, full data are in the supporting information.

The number of PS1 residues forming β-sheet varies from 0 to ~6, the upper limit corresponding to the experimental structure (**Fig. 4, row 2, S4e** and **Tables 1, S2**). In the upper limit, three residues form β1 strand (I287, Y288, and S289) and three form β2 (K380, L381, G382), together producing an anti-parallel β-sheet, in full accordance with 6IYC. However, the tendency of the ensembles to show this situation only in the upper limit indicates that either 6IYC was modeled for the state with high sheet content or the mutant in 6IYC enforces stronger C83 binding (as required to obtain the structure in the first place). We note that recent computations suggest that inhibitors also interact with the sheet. However, since the inhibitor

was placed close to the sheet in 6IYC, MD probably preserves this motif; it would be interesting to see if a similar sheet motif could be observed by explicit de novo binding, since the apo protein has no sheet, but this has not been seen yet[53]. If the mutant differs from the wild type, it would mainly affect the experimental mutants[24] and not the present WT simulations but the temperature effect is probably similar for both the WT and mutant protein.

The analysis of the representative structures from the clustered trajectories show that either both or none of these strands is present in the structure (**Supplementary Table S9**), i.e. we show that their strand tendency is strongly dependent on each other and thus highly correlated, which partly explains their delicate stability. In the cold and cooled membrane states, one seed maintained a constant number (six) of β-sheet residues throughout the equilibrated trajectory, which however reflects the 6IYC state without thermal hot state equilibration. We conclude that this structural state was modeled specifically when building the 6IYC coordinates, and our analysis supports it as a minor, not major, conformation in the hot wild-type.

Important interactions affected by cooling and membrane

One of the most important structural properties of γ-secretase is the distance between the catalytic Asp257 and Asp385 residues of PS1[54–59], conveniently analyzed via the distance between their Cα-atoms. The distance defines the open, semi-open, and closed conformation states of γ-secretase according to the FIST model[45,46], where the semi-open state provides the strongest substrate affinity and longest retention time of C99, and thus trims it down to shorter peptides (e.g. $A\beta_{40}$), whereas the open state binds more weakly and produces imprecise cleavage releasing the longer peptide $A\beta_{42}$. This model lends experimental support from the finding that distinct PS1 mutations reduce the enzyme-substrate complex stability[60].

Fig. 5 and **Table 1** (**Supplementary Fig. S4f** and **Table S2)** summarize the Asp257-Asp385 distances. The experimental 6IYC distance is 1.06 Å, shown as blue dashed lines. In all ensembles except the hot water state, the distance is typically ~1.06−1.2 nm. As shown above, the cryo-contraction in the experimental structure affects the coordinates, and a uniform coordinate scaling by 1.01, based on the R_g contraction, seems reasonable. Such scaling would change the experimental 1.06 Å to 1.11 Å, excellently centered in the middle of the dynamic range of all the membrane simulations (**Fig. 5a, 5b, 5c**). Interestingly, in the hot water state **(Fig. 5d),** this distance expands to a broad dynamic range of 1.3−1.7 nm, i.e. the membrane brings the two catalytic aspartates substantially closer together, a necessary structure-function

relationship of this and related membrane proteases. Thus, while the membrane expands the general protein ensemble, as measured by average R_g and SASA (**Fig. 2**), it brings the catalytic aspartates much closer at the same time. This tight membrane control of the short optimal Asp-Asp distance is well understood by the FIST model where pathogenic PS1 mutations favor the open state by increasing this average distance. Comparison to the cold water state (**Fig. 5e**) shows that cryo-temperature also enforces a short distance, i.e. the membrane exerts a cooling effect on the Asp-Asp structural dynamics that counteracts the temperature-favored open, pathogenic conformation state of γ-secretase.

We also found that the number of C83-PS1 hydrogen bonds are generally larger in the membrane than in water for the hot state (**Fig. 5, row 2, Fig. S4g** and **Table 1**, **Table S2**). The number varies greatly at ambient temperature due to the continuous reversible formation and breaking of these weak bonds by thermal energy. Again, it is evident that the membrane plays a central role in the protein's function, in this case by favoring stronger substrate-PS1 interactions than seen in water. The experimental structure likely represents a mixture of these two cases (nine hydrogen bonds in 6IYC minimized structure after hydrogen addition, calculated by DSSP) [24]. The cooled and cold states showed similar behavior with a constant number of hydrogen bonds. The hydrogen bonding of C83 with other subunits is summarized in **Supplementary Fig. S9**.

Fig. 6 (further details in **Supplementary Table S10**) highlights the main structural and dynamic features of the different thermal states of the protein in both membrane and water. In general, we find that the cooled state is in close agreement with the experimental 6IYC state and clearly distinct from the other states, as expected because the cooling rate is finite and the sample represents a mixture of lipid and water composition. Many of the structural parameters, in particular the water density and general membrane structure and Asp257-Asp385 distance, are similar to the hot state. We importantly identify two conformations of C83 bound to γ-secretase with different extent of helix unwinding, with only the most unwound state seen in 6IYC. The PS1 β-sheet content for one of our seeds was comparable to 6IYC, but it represents a maximum in the ensemble which is not clear from the paper[24].

In two very important ways the cooled protein differs from the hot membrane protein: By a general cryo-contraction of 1% in R_g, and a corresponding reduction in SASA, which consistently lie between the hot and cold states. The dynamics of the cooled state, as measured by RMSD, and RMSF, and the general free energy landscapes, resembles closely the cold state. From the combined results, the experimental 6IYC is clearly a compositional mixture of water

and lipid-like system with properties in-between the hot and cold state, but closest to the cooled complete membrane state with infinite cooling rate. The short Asp-Asp distance of 6IYC is most likely due to the mutation that enforces C83 binding.

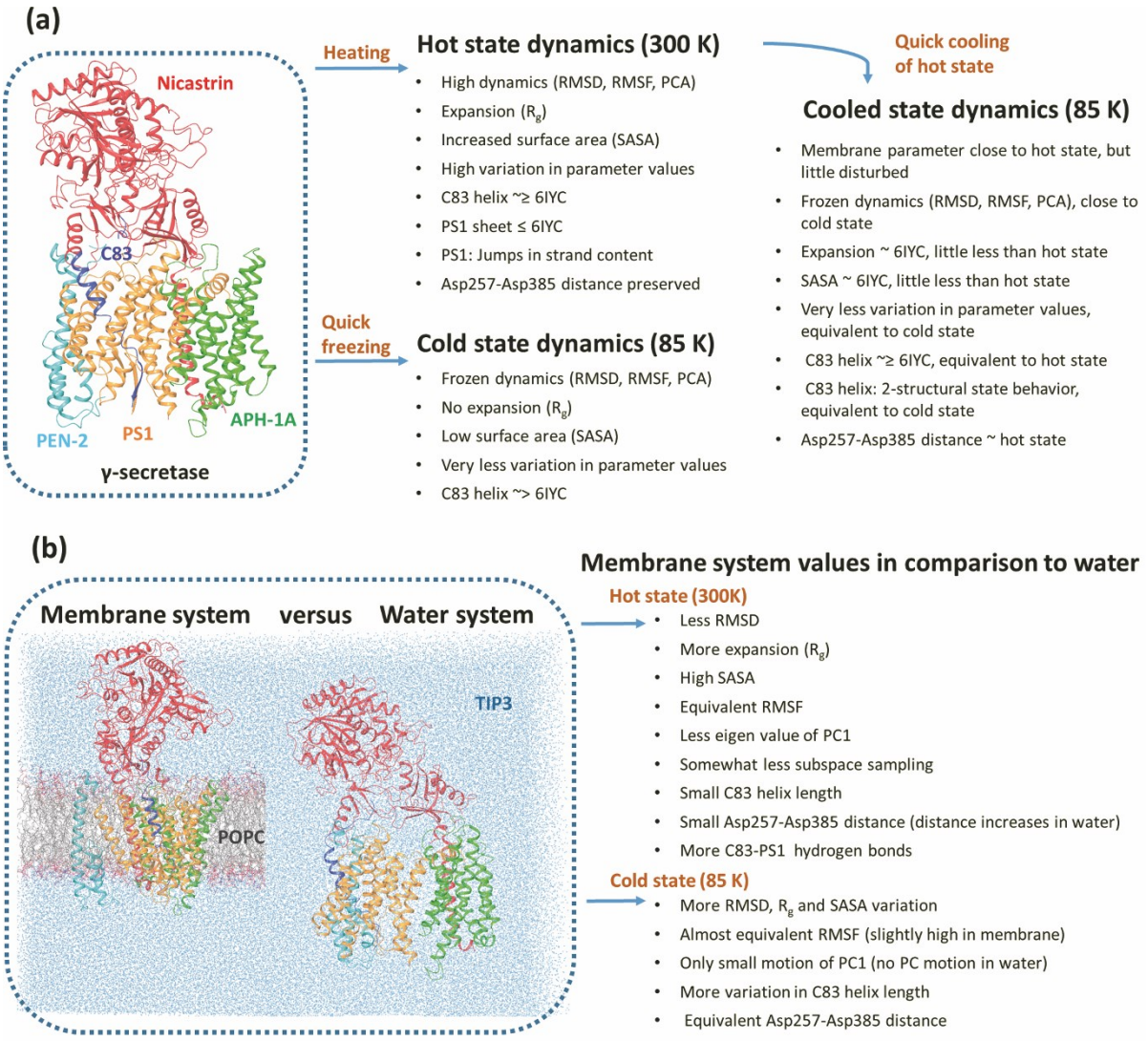

Fig. 6 Summary of the study and findings. (a) Hot versus cold state dynamics in both membrane and water systems and the resemblance of the cooled state with the hot or cold states in membrane. **(b)** Membrane versus water system dynamics in both hot and cold states.

Cryo-EM can potentially use random pictures of many independent molecules to sample the conformation space, but the number needs to be so large that the small Boltzmann populations of these states are represented, and still then they may be poorly modeled due to their low partial density. While we propose that uniform coordinate scaling can uniformly

correct cryo-structure coordinates for the cryo-contraction based on MD simulations of the type proposed here, the protein-specific conformational ensembles that are important to function need MD simulation at the hot state regardless. It is not surprising, considering current cooling rates of milliseconds per degree or slower, that most protein modes except major conformational changes are frozen out in a single cryo-EM image. This phenomenon has been well-documented in the case of residue side chain conformations e.g. by Linden et al. using cooling rates of 10°C per second[9].

Any non-uniform correction to the conformational states enforced by changed protein hydration are protein-specific; in the case of γ-secretase, the cooled state, even at infinite cooling rate as studied here, has lost all conformational states that are not the global minimum of the free energy landscape. For γ-secretase in particular, this prevents the direct testing of our prediction that γ-secretase has three conformation states affecting the substrate-binding site at ambient temperature, as only the most stable of these states is seen in the cryo-EM data, yet we argue that these multiple states are required to explain the diverse cleavage patterns of Aβ.

Since the $A\beta_{42}/A\beta_{40}$ ratio correlates with disease onset[61] (a previous analysis suggested it did not [62] but reexamination of the data shows so[61]), this ratio is very important to AD and the structure-function relationship causing this ratio is explained by the FIST model: Accordingly, PS1 mutations favor the open conformation by destabilizing the protein conformation and hydrophobic packing, thus releasing the peptides earlier at higher $A\beta_{42}/A\beta_{40}$ ratio[45,63]. In contrast, γ-secretase modulators that reduce $A\beta_{42}/A\beta_{40}$ ratios probably act by contributing their binding affinity to the stability of the C99-γ-secretase complex[64–70].

Conclusions

We asked the question how cryo-EM structures differ from the hot state and the cold state of the same protein, and how membrane and water contributes to these differences. As far as we know this is the first detailed study of this kind; It is hard to perform experimentally because samples are damaged by radiation at high temperature, and adequate pure membrane and water control systems cannot currently be constructed experimentally as done here. Thus, some of our findings are mainly predictions. However, the consistent agreement between our simulated cooled state and the experimental structure and the tendency of temperature effects to be well-modeled by MD, and the close similarity of our observed cryo-contraction to similar effects seen in a few other experimental studies of other proteins, strongly speak for at least the qualitative truth of our findings.

We show clearly that the published structure 6IYC represents a cryo-contracted state with important conformations frozen out. We estimate that the radius of gyration and the solvent accessible surface area of the protein should be approximately 1% larger at room temperature and suggest a uniform scaling of all the structural 6IYC coordinates by 1.01 to correct for this phenomenon. The cryo-contraction is particularly large for γ-secretase because of its large non-spherical structure with many flexible parts, notably nicastrin and the PS1 loops. We also show that the contraction is much larger in the membrane than in water, and thus the hot state in the membrane requires a larger rescaling of the structural cryo-EM coordinates.

Our simulated cooled structure resembles closely the experimental 6IYC structure, in particular considering that this structure is a mixture of the full membrane and full water systems (**Table 1, Fig. 2**). However, cooled state dynamics are "cold", i.e. similar to that of the cold state (RMSD, RMSF, PCA) and thus, its free energy landscape represents the freezing out of almost all important modes of the protein (**Fig. 3**). In terms of structural properties, the cooled state and experimental 6IYC structure resemble a mixture of the hot and cold state, as seen from the deuterium order parameters, the water density, the radius of gyration, and solvent-accessible surface area.

Our study also casts important light on the role of the membrane in controlling the structure and dynamics of this important membrane protease. Previous work has shown that the membrane composition affects the dynamics and function of γ-secretase.[50–52] Although our interest here was mainly to separate out the thermal effects, both thermal and membrane effects are clearly important for γ-secretase dynamics. We find that the membrane reduces structural variation but enhances the thermal differences and substantially affects the functional dynamics of γ-secretase. Two important conformations in the substrate-binding pocket freeze out in the experimental cooled sample. Our simulated cooled protein contains both an unwound C83-substrate with 10-14 α-helix residues (6IYC: 11) and an intact state with 16 helix residues not reported in the cryo-EM structure. The difference with the cryo-EM structure might be due to the force field artefacts. However, these conformations may explain the different retention time and substrate cleavage leading to different Aβ peptides, notably $A\beta_{42}$ and $A\beta_{40}$ considered central to Alzheimer's disease. The loosely bound conformation of the hot state is probably responsible for the imprecise cleavage and earlier release of longer Aβ peptides, whereas the compact state keeps the substrate for longer, in good agreement with the FIST model[45,46].

In terms of the much debated β-sheet recognition motif, we find that it is completely reproduced in our cooled state but is only transient at room temperature due to thermal

unzipping. Indeed, when using the state-of-the-art DSSP algorithm (implemented in Gromacs 2018.5), the sheet between APP-C83 and PS1 does not exist even in 6IYC itself. Only some programs conclude that such a sheet exists in 6IYC (e.g. PyMOL). Thus, the signal is very weak, consistent with our finding that it represents a minor populated state favored in the model building, with the uncertainty in the backbone torsion angles preventing DSSP recognition. It is thus an open question whether this sheet exists for the natural substrate APP-C99 as it binds more weakly than APP-C83 and this obviously warrants further investigation.

Very large ensembles of cryo-EM images for thousands of distinct protein molecules are required to cover the small Boltzmann weights of important conformations aside from the conformation lowest in free energy, resulting in "partial densities" (resembling "partial occupations" in X-ray structures[4]. This is particularly true since most cryo-EM-relevant proteins have functionally important conformational modes at timescales faster than the cooling rate. MD simulations produce fully Boltzmann-weighted free energy landscapes directly. The added advantage of being able to correct the differences between the cooled and hot states makes MD a promising, if not essential, supplement to multi-particle reconstruction in cryo-EM, as shown in the present paper.

Conflicts of interest

The authors declare no conflict of interest.

Acknowledgements

The Danish Council for Independent Research | Natural Sciences (DFF), grant case 7016-00079B, is acknowledged for supporting this work.

Supporting Information

The supporting file contains information about system set-up, membrane, water and protein parameters, R_g and SASA of each subunit of γ-secretase and correlation between them, average and standard deviation of protein properties, clustering of equilibrated trajectories, PS1 β-strand analysis, RMSF plots and C83 interactions with other system subunits.

References

1 R. Fernandez-Leiro and S. H. W. Scheres, *Nature*, 2016, 537, 339–346.

2 X.-C. Bai, G. McMullan and S. H. W. Scheres, *Trends Biochem. Sci.*, 2015, **40**, 49–57.

3 K. Murata and M. Wolf, *Biochim. Biophys. Acta - Gen. Subj.*, 2018, 1862, 324–334.

4 D. Elmlund and H. Elmlund, *Annu. Rev. Biochem.*, 2015, **84**, 499–517.

5 A. Meents, S. Gutmann, A. Wagner and C. Schulze-Briese, *Proc. Natl. Acad. Sci.*, 2010, **107**, 1094–1099.

6 T. Althoff, D. J. Mills, J. L. Popot and W. Kühlbrandt, *EMBO J.*, 2011, **30**, 4652–4664.

7 J. Frauenfeld, R. Löving, J. P. Armache, A. F. P. Sonnen, F. Guettou, P. Moberg, L. Zhu, C. Jegerschöld, A. Flayhan, J. A. G. Briggs, H. Garoff, C. Löw, Y. Cheng and P. Nordlund, *Nat. Methods*, 2016, **13**, 345–351.

8 T. H. Bayburt and S. G. Sligar, *FEBS Lett.*, 2010, 584, 1721–1727.

9 A. H. Linden, W. T. Franks, Ü. Akbey, S. Lange, B. J. Van Rossum and H. Oschkinat, *J. Biomol. NMR*, 2011, **51**, 283–292.

10 R. F. Tilton Jr, J. C. Dewan and G. A. Petsko, *Biochemistry*, 1992, **31**, 2469–2481.

11 W. Doster, A. Bachleitner, R. Dunau, M. Hiebl and E. Lüscher, *Biophys. J.*, 1986, **50**, 213–219.

12 K. V Dunlop, R. T. Irvin and B. Hazes, *Acta Crystallogr. Sect. D Biol. Crystallogr.*, 2005, **61**, 80–87.

13 X. Bai, E. Rajendra, G. Yang, Y. Shi and S. H. Scheres, *Elife*, 2015, **4**, 551–560.

14 A. Twomey, K. Kurata, Y. Nagare, H. Takamatsu and A. Aksan, *Int. J. Pharm.*, 2015, **487**, 91–100.

15 G. Petzold and J. M. Aguilera, *Food Biophys.*, 2009, **4(4)**, 378–396.

16 J. Dong, A. Hubel, J. C. Bischof and A. Aksan, *J. Phys. Chem. B*, 2009, **113**, 10081–10087.

17 T. Sei, T. Gonda and Y. Arima, *J. Cryst. Growth*, 2002, **240**, 218–229.

18 H. Zhang, I. Hussain, M. Brust, M. F. Butler, S. P. Rannard and A. I. Cooper, *Nat. Mater.*, 2005, **4**, 787–793.

19 A. Twomey, R. Less, K. Kurata, H. Takamatsu and A. Aksan, *J. Phys. Chem. B*, 2013, **117**, 7889–7897.

20 E. K. Bigg, *Proc. Phys. Soc. Sect. B*, 1953, **66**, 688.

21 M. Karplus and J. A. McCammon, *Nat. Struct. Biol.*, 2002, **9**, 646–652.

22 D. H. Juers and B. W. Matthews, *Q. Rev. Biophys.*, 2004, **37**, 105–119.

23 X. Bai, C. Yan, G. Yang, P. Lu, L. Sun, R. Zhou, S. H. W. Scheres and Y. Shi, *Nature*, 2015, **525**, 212–218.

24 R. Zhou, G. Yang, X. Guo, Q. Zhou, J. Lei and Y. Shi, *Science* 2019, **363**, eaaw0930.

25 G. Yang, R. Zhou, Q. Zhou, X. Guo, C. Yan, M. Ke, J. Lei and Y. Shi, *Nature*, 2019, **565**, 192–197.

26 D. S. BIOVIA, Discovery Studio Modeling Environment, Release 2017, San Diego.

27 G. Vriend, *J. Mol. Graph.*, 1990, **8(1)**, 52–56.

28 W. . . DeLano, *CCP4 Newsl. Protein Crystallogr.*, 2002, **40(1)**, 82–92.

29 M. A. Lomize, I. D. Pogozheva, H. Joo, H. I. Mosberg and A. L. Lomize, *Nucleic Acids Res.*, 2012, **40**, D370–D376.

30 S. Jo, T. Kim, V. G. Iyer and W. Im, *J. Comput. Chem.*, 2008, **29**, 1859–1865.

31 X. Cheng, J. B. Klauda, S. Jo, D. A. Case, J. C. Jeong, J. A. Lemkul, V. S. Pande, J. M. Swails, Y. Qi, P. K. Eastman, W. Im, C. L. Brooks, J. Lee, S. Wei, A. D. MacKerell, M. S. Yeom and J. Buckner, *J. Chem. Theory Comput.*, 2015, **12**, 405–413.

32 D. Van Der Spoel, E. Lindahl, B. Hess, G. Groenhof, A. E. Mark and H. J. C. Berendsen, *J. Comput. Chem.*, 2005, **26**, 1701–1718.

33 H. J. C. Berendsen, D. van der Spoel and R. van Drunen, *Comput. Phys. Commun.*, 1995, **91**, 43–56.

34 H. J. C. Berendsen, J. P. M. Postma, W. F. van Gunsteren, A. DiNola and J. R. Haak, *J. Chem. Phys.*, 1984, **81**, 3684–3690.

35 J. B. Klauda, R. M. Venable, J. A. Freites, J. W. O'Connor, D. J. Tobias, C. Mondragon-Ramirez, I. Vorobyov, A. D. MacKerell and R. W. Pastor, *J. Phys. Chem. B*, 2010, **114**, 7830–7843.

36 W. L. Jorgensen, J. Chandrasekhar, J. D. Madura, R. W. Impey and M. L. Klein, *J. Chem. Phys.*, 1983, **79**, 926.

37 D. J. Evans and B. L. Holian, *J. Chem. Phys.*, 1985, **83(8)**, 4069–4074.

38 X. Daura, K. Gademann, B. Jaun, D. Seebach, W. F. Van Gunsteren and A. E. Mark, *Angew. Chemie Int. Ed.*, 1999, **38**, 236–240.

39 M. Parrinello and A. Rahman, *J. Appl. Phys.*, 1981, **52**, 7182–7190.

40 L. Verlet, *Phys. Rev.*, 1967, **159**, 98–103.

41 S. Páll and B. Hess, *Comput. Phys. Commun.*, 2013, **184**, 2641–2650.

42 S. Buchoux, *Bioinformatics*, 2017, **33**, 133–134.

43 J. Seelig and J. L. Browning, *Febs Lett.*, 1978, **92**, 41–44.

44 B. Dehury, N. Tang and K. P. Kepp, *Biochem. J.*, 2019, **476**, 1173–1189.

45 A. K. Somavarapu and K. P. Kepp, *ACS Chem. Neurosci.*, 2017, **8**, 2424–2436.

46 A. K. Somavarapu and K. P. Kepp, *Neurobiol. Dis.*, 2016, **89**, 147–156.

47 P. Robustelli, S. Piana and D. E. Shaw, *Proc. Natl. Acad. Sci. U. S. A.*, 2018, **115**, E4758–E4766.

48 R. Mehra and K. P. Kepp, *J. Chem. Phys.*, 2019, **151**, 85101.

49 A. K. Somavarapu and K. P. Kepp, *ChemPhysChem*, 2015, **16**, 3278–3289.

50 R. Aguayo-Ortiz, C. Chávez-García, J. E. Straub and L. Dominguez, *Chem. Sci.*, 2017, **8**, 5576–5584.

51 M. Audagnotto, A. K. Lorkowski and M. Dal Peraro, *Biochem. Biophys. Res. Commun.*, 2018, **498**, 334–341.

52 R. Aguayo-Ortiz, J. E. Straub and L. Dominguez, *Phys. Chem. Chem. Phys.*, 2018, **20**, 27294–27304.

53 M. Hitzenberger and M. Zacharias, *ACS Chem. Neurosci.*, 2019, **10**, 3398–3403.

54 D. B. Northrop, *Acc. Chem. Res.*, 2001, **34**, 790–797.

55 E. Erez, D. Fass and E. Bibi, *Nature*, 2009, 459, 371–378.

56 A. Tolia, L. Chávez-Gutiérrez and B. De Strooper, *J. Biol. Chem.*, 2006, **281**, 27633–27642.

57 X. Li, S. Dang, C. Yan, X. Gong, J. Wang and Y. Shi, *Nature*, 2013, **493**, 56–61.

58 F. Sussman, M. C. Villaverde, J. L. Dominguez and U. H. Danielson, *Curr. Pharm. Des.*, 2013, **19**, 4257–4275.

59 R. Aguayo-Ortiz, D. C. Guzmán-Ocampo and L. Dominguez, *ChemMedChem*, 2019, **14**, 1005–1010.

60 M. Szaruga, B. Munteanu, S. Lismont, S. Veugelen, K. Horré, M. Mercken, T. C. Saido, N. S. Ryan, T. De Vos, S. N. Savvides, R. Gallardo, J. Schymkowitz, F. Rousseau, N. C. Fox, C. Hopf and B. De Strooper, *Cell*, 2017, **170**, 443–456.

61 N. Tang and K. P. Kepp, *J. Alzheimer's Dis.*, 2018, **66**, 939–945.

62 L. Sun, R. Zhou, G. Yang and Y. Shi, *Proc. Natl. Acad. Sci.*, 2016, **114**, E476–E485.

63 A. K. Somavarapu and K. P. Kepp, *J. Neurochem.*, 2016, **137**, 101–111.

64 N. Tang, A. K. Somavarapu and K. P. Kepp, *ACS Omega*, 2018, **3**, 18078–18088.

65 C. J. Crump, D. S. Johnson and Y. M. Li, *Biochemistry*, 2013, **52**, 3197–3216.

66 K. Takeo, S. Tanimura, T. Shinoda, S. Osawa, I. K. Zahariev, N. Takegami, Y. Ishizuka-Katsura, N. Shinya, S. Takagi-Niidome, A. Tominaga, N. Ohsawa, T. Kimura-Someya, M. Shirouzu, S. Yokoshima, S. Yokoyama, T. Fukuyama, T. Tomita and T. Iwatsubo, *Proc. Natl. Acad. Sci.*, 2014, **111**, 10544–10549.

67 C. J. Crump, B. A. Fish, S. V. Castro, D. M. Chau, N. Gertsik, K. Ahn, C. Stiff, N. Pozdnyakov, K. R. Bales, D. S. Johnson and Y. M. Li, *ACS Chem. Neurosci.*, 2011, **2**, 705–710.

68 Y. Ohki, T. Higo, K. Uemura, N. Shimada, S. Osawa, O. Berezovska, S. Yokoshima, T. Fukuyama, T. Tomita and T. Iwatsubo, *EMBO J.*, 2011, **30**, 4815–4824.

69 A. Ebke, T. Luebbers, A. Fukumori, K. Shirotani, C. Haass, K. Baumann and H. Steiner, *J. Biol. Chem.*, 2011, **286**, 37181–37186.

70 K. Uemura, K. C. Farner, T. Hashimoto, N. Nasser-Ghodsi, M. S. Wolfe, E. H. Koo, B. T. Hyman and O. Berezovska, *Nat. Commun.*, 2010, **1**, 130.